PCCP

PAPER

View Article Online
View Journal | View Issue

Check for updates

Cite this: Phys. Chem. Chem. Phys., 2021, 23, 11944

Active particle diffusion in convection roll arrays

Pulak Kumar Ghosh,[a] Fabio Marchesoni,*[bc] Yunyun Li*[b] and Franco Nori[de]

Received 11th March 2021,
Accepted 10th May 2021

DOI: 10.1039/d1cp01088c

rsc.li/pccp

Undesired advection effects are unavoidable in most nano-technological applications involving active matter. However, it is conceivable to govern the transport of active particles at the small scales by suitably tuning the relevant advection and self-propulsion parameters. To this purpose, we numerically investigated the Brownian motion of active Janus particles in a linear array of planar counter-rotating convection rolls at high Péclet numbers. Similarly to passive particles, active microswimmers exhibit advection enhanced diffusion, but only for self-propulsion speeds up to a critical value. The diffusion of faster Janus particles is governed by advection along the array's edges, whereby distinct diffusion regimes are observed and characterized. Contrary to passive particles, the relevant spatial distributions of active Janus particles are inhomogeneous. These peculiar properties of active matter are related to the combined action of noise and self-propulsion in a confined geometry and hold regardless of the actual flow boundary conditions.

1 Introduction

The diffusion of a tracer (organic or artificial, alike) in a suspension fluid is a standard problem of classical transport theory.[1] This paper combines two distinct aspects of this phenomenon, which recently attracted widespread inter-disciplinary interest, each for its own merit: (i) the persistent (or time-correlated) random motion of self-propelling particles and (ii) colloidal dispersion in laminar flows.

The most tractable example of persistent Brownian motion is represented by artificial micro-swimmers, namely tiny Brownian particles capable of self-propulsion in an active medium.[2,3] Such particles are designed to harvest environmental energy and convert it into kinetic energy. A class of artificial swimmers widely investigated in the current literature is the so-called Janus particles (JP), mostly spherical colloidal particles with two differently coated hemispheres, or "faces". Their axial propulsion is sustained by the dipolar near-flow-field they generate by interacting with the surrounding active (mostly highly viscous) medium. Indeed, depending on their operating conditions, JPs can induce either concentration gradients, by catalyzing some chemical reaction on their active surface, or thermal gradients, by inhomogeneous light absorption (self-thermophoresis) or magnetic excitation (magnetically induced self-thermophoresis).[4,5] Moreover, experiments demonstrated their ability to perform guided motions through periodic arrays.[6]

Recently, artificial micro- and nano-swimmers of this class have been the focus of pharmaceutical (*e.g.*, smart drug delivery[7]) and medical research (*e.g.*, robotic microsurgery[8]). These peculiar Brownian particles change direction randomly as usual, but with finite time scale; persistence makes their diffusion extremely sensitive to geometric confinement and other constraints.[9–12] Technological applications involving sub-millimeter artificial swimmers thus require accurate control of their diffusive properties in non-homogeneous environments.[1,6]

On the other hand, Brownian diffusion in an advective medium is also a nanotechnological issue, for instance, in the design and operation of microfuidic devices[13–15] or chemical reactors.[16] We consider for simplicity a Brownian tracer of free diffusion constant D_0, advected by a planar stationary laminar flow, like in Fig. 1(a). Let the velocity field of the suspension fluid be formulated as,[17] $\vec{v}_\psi = (\partial_y, -\partial_x)\psi$, where

$$\psi(x,y) = (U_0L/2\pi)\sin(2\pi x/L)\sin(2\pi y/L), \tag{1}$$

is a stream function extensively studied in the context of Rayleigh–Bénard convection.[18] On combining the two constants, L, the flow's spatial period, and U_0, the maximum advection speed, one defines the advection diffusion scale, $D_L = U_0L/2\pi$, and the maximum roll vorticity, $\Omega_L = 2\pi U_0/L$ (Appendix A).

[a] Department of Chemistry, Presidency University, 86/1 College Street, Kolkata 700073, India
[b] Center for Phononics and Thermal Energy Science, School of Physics Science and Engineering, Tongji University, Shanghai 200092, People's Republic of China. E-mail: fabio.marchesoni@pg.infn.it, yunyunli@tongji.edu.cn
[c] Dipartimento di Fisica, Università di Camerino, I-62032 Camerino, Italy
[d] Theoretical Quantum Physics Laboratory, RIKEN Cluster for Pioneering Research, Wako-shi, Saitama 351-0198, Japan
[e] Department of Physics, University of Michigan, Ann Arbor, Michigan 48109-1040, USA

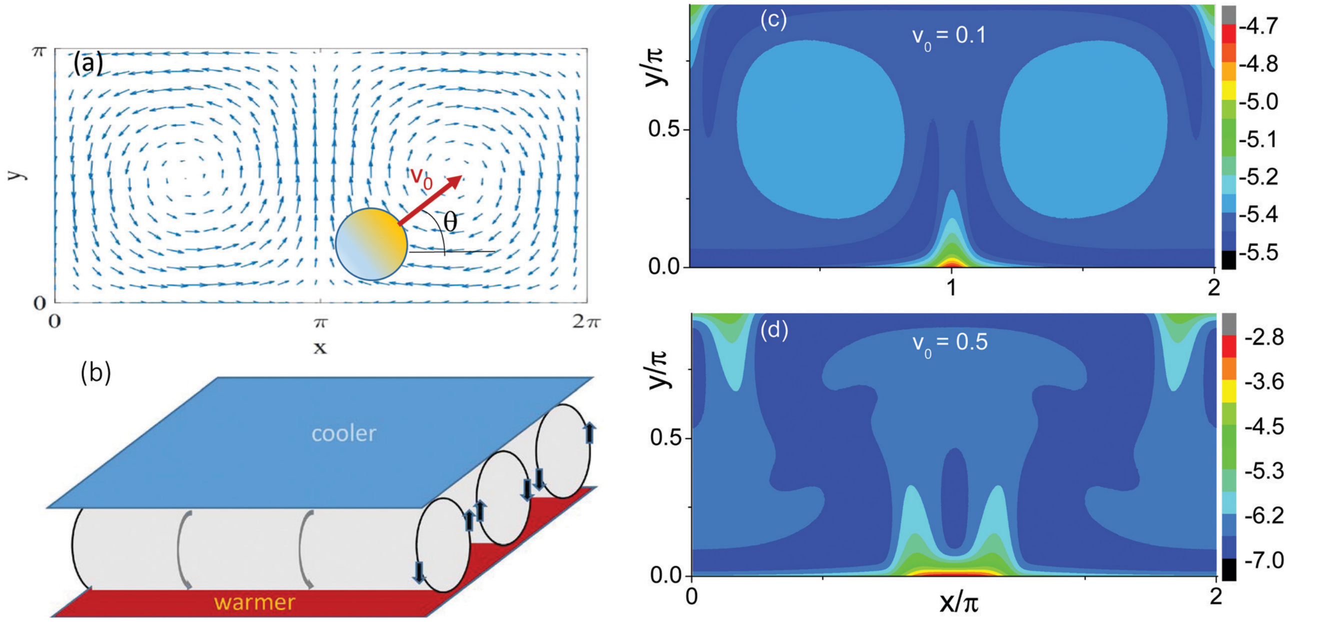

Fig. 1 Spatial distributions of a Janus particle in the laminar flow of eqn (1), sketched in (a) and (b), for v_0 = 0.1 (c) and 0.5 (d). The chart levels are color-coded on natural logarithmic scales as indicated. Other simulation parameters are: D_0 = 0.01, D_θ = 0.01, U_0 = 1 and $L = 2\pi$. According to eqn (3), here v_c = 0.4. A practical realization of a linear convection array is represented by the Rayleigh–Bénard rolls sketched in (b); the JP self-propulsion model of eqn (2) is illustrated in (a).

At high Péclet numbers, Pe = $D_L/D_0 \gg 1$, a passive tracer undergoes normal diffusion with enhanced diffusion constant $D = \kappa\sqrt{D_L D_0}$ with κ = 1.07, that is $D > D_0$.[19] This advection effect, termed advection enhanced diffusivity (AED), has been explained[19–22] by noticing that for $D_0 < D_L$ an unbiased particle jumps between convection rolls while being advected along their separatrices. Narrow flow boundary layers (FBL) of estimated width $\delta = (D_0/\Omega_L)^{1/2}$, form a network of advection channels centered around the $\psi(x,y)$ cell separatrices, thus enabling a large-scale particle's diffusion.

Peculiar effects due to the combination of self-propulsion and advection are expected to emerge when one considers an active JP suspended in a one dimensional (1D) array of counter-rotating convection rolls. An ideal experimental setup is sketched in Fig. 1(b). An array of stationary Rayleigh–Bénard cells can occur in a plane horizontal layer of fluid heated from below.[23,24] Assuming that they are counter-rotating cylinders parallel to the z-axis, the z coordinate of a suspended tracer is ignorable; hence the reduced two dimensional (2D) flow pattern of eqn (1). Advection enhanced diffusivity of passive colloidal particles in arrays of Rayleigh–Bénard rolls[18] has already been demonstrated experimentally.[25,26] Experimental data on the dispersion of self-propelling microswimmers in convective laminar flows are scarce. Recent reports mostly addressed the hydrodynamic effects of laminar flows on the self-propulsion of finite-size microswimmers of various geometries,[27] either artificial[28] or of biological nature.[29,30] In this regard, active JPs are ideal tracers for this kind of measurements because their shape and size minimize hydrodynamic effects and their self-propulsion speed can be conveniently tuned with respect to the advection drag established in the convection cell.

This paper is organized as follows. In Section 2 we present our model and briefly discuss the dynamical significance of the relevant parameters. Our derivation of the relevant time scales is detailed in Appendix A. Our main numerical results are analysed in Sections 3 and 4, where we show that: (i) the interplay of advection and self-propulsion causes the nonuniform spatial distribution of a confined active JP. For self-propulsion speeds below a certain threshold, its distribution tends to accumulate along the roll boundaries (Section 3 and Appendix B); (ii) under these conditions, its self-propulsion and advection velocities tend to line up, so that, contrary to the 2D case of ref. 31, the large-scale diffusion of an active JP is insensitive to self-propulsion itself (Section 4); (iii) active tracers with self-propulsion speeds larger than the above threshold, attain a maximum diffusion constant for an optimal persistence time, which we relate to advection at the array's edges (Section 4 and Appendix C). In Section 5 we stress the role of geometric confinement on the diffusion properties of an active JP in a convection array and show that the picture above holds also for rigid (*i.e.*, no-slip) edge flows.

2 Model

By (linear) convection array we mean here a stationary laminar flow with periodic stream function like $\psi(x,y)$ of eqn (1), confined between two parallel edges, $y = 0$ and $y = L/2$, which act as dynamical reflecting boundaries. The unit cell of the array consists of two counter-rotating convection rolls [Fig. 1(a)]. The dynamics of an overdamped active JP can then be formulated by means of two translational and one rotational Langevin equation (LE),

$$\dot{\vec{r}} = \vec{v}_\psi + \vec{v}_0 + \sqrt{D_0}\xi(t)$$
$$\dot{\theta} = (\alpha/2)\nabla\times\vec{v}_\psi + \sqrt{D_\theta}\xi_\theta(t), \quad (2)$$

where $\vec{r} = (x,y)$, $\vec{v}_\psi$ is the advection velocity introduced above, and the self-propulsion vector, $\vec{v}_0 = v_0(\cos\theta,\sin\theta)$, has constant modulus, v_0, and is oriented at an angle θ with respect to the longitudinal x-axis. The translational (thermal) noises in the x and y directions, $\xi(t) = (\xi_x(t),\xi_y(t))$, and the rotational noise, $\xi_\theta(t)$, are stationary, independent, delta-correlated Gaussian noises, $\langle\xi_i(t)\xi_j(0)\rangle = 2\delta_{ij}\delta(t)$, with $i,j = x,y,\theta$. D_0 and D_θ are the respective noise strengths, which for generality we assume to be unrelated.[10] To avoid uncontrolled hydrodynamic effects, the particle is taken to be pointlike.[15] Other effects due to its actual geometry and chemical-physical characteristics are encoded in the model dynamical parameters. The reciprocal of D_θ coincides with the angular persistence (or correlation) time, τ_θ, of $\vec{v}_0$; accordingly, $l_\theta = v_0/D_\theta$ quantifies the persistence length of the particle's self-propelled random motion. The flow shear exerts a torque on the particle proportional to the local fluid vorticity, $\nabla\times\vec{v}_\psi$.[31,32] For simplicity, we adopt Faxén's second law, which, for an ideal no-stick spherical particle, yields $\alpha = 1$.[33] In the high Péclet number regime addressed here, Pe $\gg$ 1 or $D_0 \ll D_L$, particle diffusion is strongly influenced by advection (Appendix A).

The Langevin eqn (2) can be conveniently reformulated in dimensionless units by rescaling $(x,y)\to(\tilde{x},\tilde{y}) = (2\pi/L)(x,y)$ and $t \to \tilde{t} = \Omega_L t$. The three remaining independent parameters get rescaled as follows: $v_0 \to v_0/U_0$, $D_0 \to D_0/D_L$ and $D_\theta \to D_\theta/\Omega_L$. This means that, without loss of generality, we can set $L = 2\pi$ and $U_0 = 1$ and the ensuing simulation results can be regarded as expressed in dimensionless units and easily scaled back to arbitrary dimensional units. The stochastic differential eqn (2) were numerically integrated by means of a standard Milstein scheme.[34] Particular caution was exerted when computing the asymptotic diffusion constant, $D = \lim_{t\to\infty}\langle[x(t) - x(0)]^2\rangle/2t$, because for low values of the noise strengths, D_0 and D_θ, the transients of the diffusion process grow exceedingly long.[32,35] For asymptotically large running times, our estimates of D are independent of the starting point $(x(0),y(0))$.

3 Spatial distributions

In sharp contrast with the noiseless limit, $D_0 = D_\theta = 0$, investigated in ref. 32, the spatial distribution of a noisy active JP is not uniform. The outcome of our numerical simulations is summarized in Fig. 1(c), (d) and 2. The laminar flow acts upon the particle through both an advection drag and an advection torque. Along the roll boundaries the drag is maximum (with speed approaching U_0, except at the "stagnation" corners), but the torque vanishes. At low self-propulsion speeds, this favours the orientation of $\vec{v}_0$ parallel to the advection velocity $\vec{v}_\psi$. The JP thus undergoes a large-scale intra-roll circulation motion, which causes its accumulation along the outer layers of the rolls. The less pronounced particle accumulation at the roll centers is attributable to the higher vorticity there.[35] These two areas of accumulation are separated by a circular depletion region. Indeed, in Fig. 1(c) and 2(a), (b) (see also Appendix B) the particle appears to be sucked in by the ascending ($x = L/2$) and descending boundary flows ($x = 0,L$), an effect that seems to increase with increasing v_0.

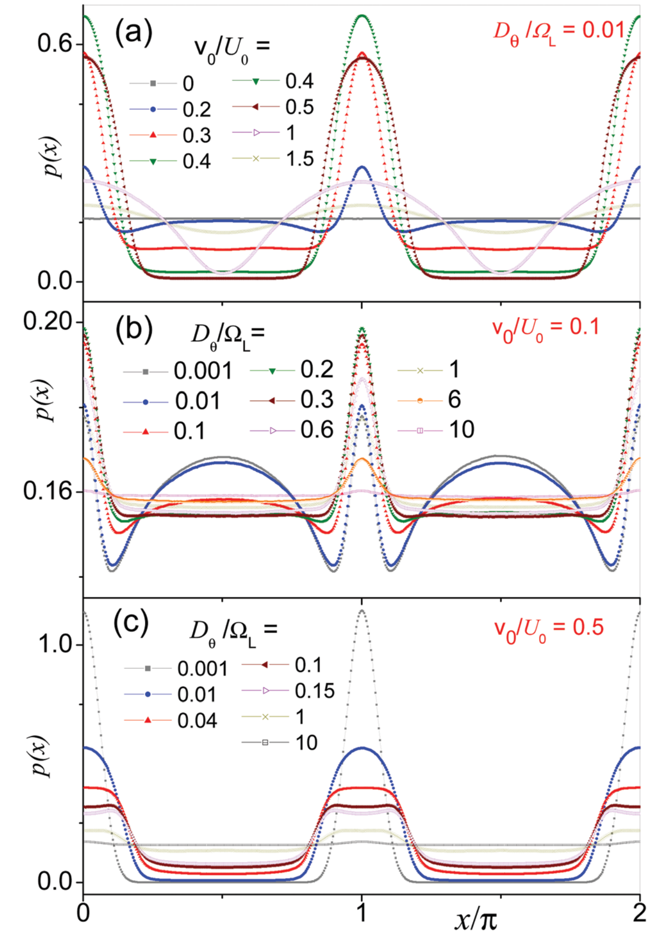

Fig. 2 Stationary longitudinal distributions, $p(x)$, of a Janus particle in the laminar flow of eqn (1) for (a) $D_\theta = 0.01$ and different v_0; (b) $v_0 = 0.1$ and (c) $v_0 = 0.5$ and different D_θ (see legends). Other simulation parameters are: $D_0 = 0.01$; $U_0 = 1$ and $L = 2\pi$, with $D_L = \Omega_L = 1$.

This picture changes abruptly as v_0 is raised above a critical value v_c [Fig. 2(a)], which we established to depend on the strength of the thermal noise, D_0 (Appendix C). The intra-roll circulation of Fig. 1(c) is suppressed and the roll interior gets depleted [Fig. 2(a) and (c)]; as a result, the particle piles up symmetrically at the base of the ascending (bottom edge) and descending flows (top edges). Moreover, for v_0U_0, the particle seems to diffuse mostly along the array's edges, which explains why the longitudinal distributions, $p(x)$, turn uniform again with increasing v_0, while the transverse distributions, $p(y)$, remain peaked at $y = 0,L/2$ (Appendix B). One also notices that the peaks of $p(x)$ widen with increasing v_0 [Fig. 2(a)] and D_θ [Fig. 2(c)].

The relevance of these results can be best appreciated by comparison with the diffusion of a passive particle in the same

1D convection array. In that case, the flow boundary layers still control the particle's large-scale diffusion, but all stationary distributions, $p(x,y)$, remain uniform.[35] This conclusion applies also to noiseless self-propelling JPs in 1D convection arrays, as proven in ref. 32, but is no longer true in the presence of thermal noise. Indeed, upon hitting either array edge, the particle will persist pointing against it for a time τ_θ; hence the angular correlation of $\vec{v}_0$ and $\vec{v}_\psi$. [Note that in most simulations presented here τ_θ is larger than the circulation characteristic time, *i.e.*, $D_\theta < \Omega_L$.] Accordingly, no probability density accumulation at the roll boundaries was detected for an active JP in the 2D laminar flow of eqn (1) with periodic boundary conditions, regardless of the noise strengths, D_0 and D_θ (Appendix B). This leads to the conclusion that the FPL structure we detected in the stationary distributions $p(x,y)$ of an active JP diffusing in a 1D convection array is a combined effect of noise and geometric confinement.

The self-propulsion threshold, v_c, can be estimated as follows. When the vector $\vec{v}_0$ points inwards, the particle pulls away from the edge a length of the order of $v_0/4\Omega_L$, before being swept into a vertical flow layer. As such length grows comparable with the width of an unbiased flow boundary layers, *i.e.*, for $v_0 > v_c$ with

$$v_c/U_0 = 4\sqrt{D_0/D_L}, \tag{3}$$

the particle exits the FBL and its circulation along the roll separatrices is interrupted. This estimate of v_c is consistent with our simulation data for $p(x)$ and $p(y)$ at low angular noise, $D_\theta \ll \Omega_L$ [compare Fig. 1 and 2; see Appendices B and C for more details]. Note, for instance, that in Fig. 2 the $p(x)$ regions delimited by the peaks at $x = 0$, π and 2π get depleted only for $v_0 = 0.5$, that is for $v_0 > v_c$. Moreover, being confined in a FBL, a JP with $v_0 < v_c$ ought to behave like a passive colloidal particle, *i.e.*, undergo advection enhanced diffusivity as an effect of the sole thermal noise. The diffusion data presented in the next section (Fig. 3) confirm this conclusion.

As the FBL circulation breaks up, the JP tends to accumulate against the array edges, provided that the self-propulsion length is larger than the array width, $l_\theta > L/2$, or, equivalently, $D_\theta/\Omega_L < v_0/U_0$. However, its motion along the edges is not advection-free. The coordinate x in eqn (2) then obeys the approximate LE, $\dot{x} = U_0\langle\cos(2\pi y/L)\rangle\sin(2\pi x/L) + v_0\cos\theta + \xi_x(t)$, which describes the dynamics of a Brownian particle pinned to a washboard potential[36] (advection term) and subjected to a colored, non-Gaussian tilting noise, $v_0\cos\theta(t)$, with correlation time τ_θ[10] (self-propulsion term). The average $\langle\cos(2\pi y/L)\rangle$ depends on all three free parameters v_0, D_θ and D_0; in particular, its modulus increases with increasing v_0 and decreasing D_θ. This simple observation explains: (i) the non-monotonic v_0-dependence of the $p(x)$ peaks, whereby a larger v_0 implies not only higher washboard potential barriers, but also a stronger tilting term; (ii) the flattening of the longitudinal distributions for v_0U_0, as self-propulsion wins over the advection pinning action at the edges; (iii) the broadening and double-peaked profile of the $p(x)$ peaks in Fig. 2(c) on increasing D_θ which is a well-known effect of colored noise.[37]

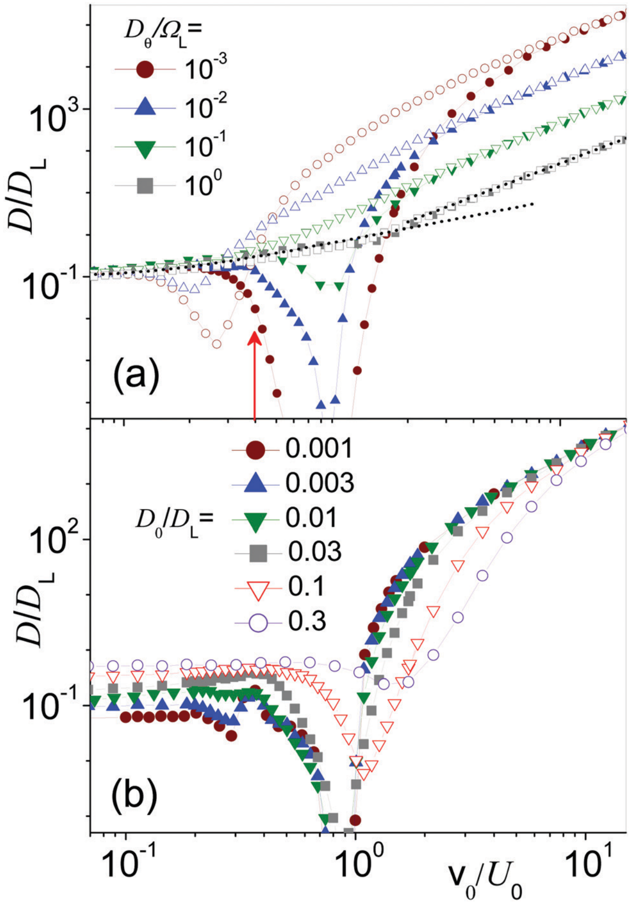

Fig. 3 (a) Longitudinal diffusion of a JP in the laminar flow of eqn (1) (solid symbols) and (5) (empty symbols): D/D_L *vs.* v_0/U_0 for D_0 = 0.01 and different D_θ (see legends). Dashed curves represent the estimates, $D = \kappa\sqrt{D_L(D_0 + D_s)}$ and $D = D_0 + D_s$, with $D_s = v_0^2/2D_\theta$, respectively, for low and high v_0 (see text). Our estimate for v_c, eqn (3), is marked by a vertical arrow. (b) D/D_L *vs.* v_0/U_0 for D_θ = 0.01 and different D_0. Flow parameters are U_0 = 1 and $L = 2\pi$, with $D_L = \Omega_L = 1$.

On increasing D_θ, the JP self-propulsion length eventually grows shorter than the roll size, $l_\theta < L/2$; the active particle then tends to behave like a passive Brownian particle, except its free diffusion constant, D_0, must be now incremented by the extra term $D_s = v_0^2/2D_\theta$. Accordingly, both its spatial distributions, $p(x)$ and $p(y)$, become uniform [see Fig. 2(b), (c) and Appendix B].

4 Longitudinal diffusion

Based on the qualitative arguments of Section 3, we expect to observe distinct diffusion regimes for a JP with $l_\theta > L/2$. Our expectation are supported by the simulation data reported in Fig. 3(a and b). Indeed, the curves D *versus* v_0 exhibit distinct behaviors for $v_0 < v_c$, $v_c < v_0U_0$ and $v_0 \gg U_0$. For $v_0 \gg U_0$, advection is negligible compared to self-propulsion; since we assumed reflecting boundaries at the array's edges, not surprisingly, $D \to D_0 + D_s$.[31] This behavior is in sharp contrast with the scenario suggested by the D curves in the limit $v_0/U_0 \to 0$. All curves overlap, insensitive to D_θ, and, more remarkably, tend to the advection enhanced diffusivity estimate, $D = \kappa\sqrt{D_L D_0}$, for passive pointlike particles.[19] Such a behavior persists for v_0 up to an upper value, which appears to agree well with our estimate for v_c in eqn (3). This picture holds also at lower thermal noise strengths, Fig. 3(b) and Appendix C (though not with as good statistics). This result confirms that for $v_0 < v_c$ the array's edges make the JP self-propulsion velocity, $\vec{v}_0$, to line up with the advection drag, $\vec{v}_\psi$, so that the JP diffuses only through the FBL network due to thermal fluctuations.

The intermediate regime, $v_c < v_0 U_0$, is characterized by a sharp drop of the particle's diffusivity. This is a signature of its pinning to the array's edges. For $D_\theta/\Omega_L \ll v_0/U_0$, the particle can slide along the edges only by overcoming the advection washboard potential of amplitude $D_L|\langle\cos(2\pi y/L)\rangle|$. In the limit of very low noises, D_0/D_L, $D_\theta/D_L \to 0$, this occurs for $v_0 \sim U_0$. For $D_0/D_L \ll \{|\langle\cos(2\pi y/L)\rangle|, v_0/U_0\}$, its diffusion constant drops to exponentially small values,[36] which could not be computed numerically. On increasing D_0 and (or) D_θ, the amplitude of the pinning potential diminishes, and the particle's diffusivity becomes numerically appreciable; eventually, the diffusion dips because pinning becomes negligible.

Interesting is the shift of the D minima to higher v_0 values with increasing D_0 (inset of Fig. 3). This counterintuitive effect, is due to the fact that for $D_\theta/\Omega_L < D_0/D_L \ll 1$, the JP self-propulsion velocity, $\vec{v}_0$, changes direction owing to the combined action of thermal noise (pulling the particle away from its pinning site) and advection (exerting a torque on it). A larger dispersion of the JP orientation angle, θ, with thermal noise, implies a higher depinning value of v_0.

We stress here, once again, the role of advection along the array's edges. In a periodic 2D convection array of stream function (1), the v_0-dependence of D is quite different.[31,32] In the noiseless limit, a spherical JP gets trapped for v_0 lower than the threshold $v_{th} \simeq 2.2\ U_0$.[32] After a generally long transient, during which it keeps roll jumping, the particle eventually ends being uniformly distributed inside a single convection roll (*i.e.*, with $v_c = 0$). Here, instead, advection at the array's edges lowers the trapping threshold down to U_0.

As anticipated above and illustrated in Fig. 4, D_θ, is an important control parameter, because it governs orientation and persistence of self-propulsion. When D_θ is so large that D_s is negligible compared to D_0, $D_\theta/\Omega_L \gg (D_L/D_0)(v_0/U_0)^2$, the passive particle regime is recovered, no matter the value of v_0. In Fig. 4 we set $D_0 < D_L$, *i.e.*, Pe $\gg$ 1: therefore, for $D_\theta/\Omega_L \to \infty$, all D curves plotted there tend to the same (high Péclet number) advection enhanced diffusivity value, $D = \kappa\sqrt{D_L D_0}$. More remarkably, the two curves with $v_0 < v_c$ only slightly deviate from that value throughout the entire D_θ domain. This result is a further evidence of the particle's confined circulation inside the FBLs.

The curves for $v_c < v_0 U_0$ overshoot the advection enhanced diffusivity value, with overlapping maxima at $D_\theta \sim \Omega_L$. This effect is due to the synchronized action of angular diffusion

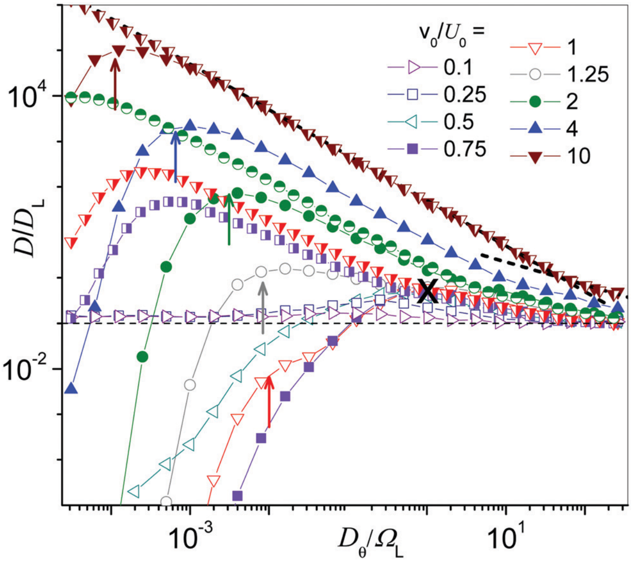

Fig. 4 Longitudinal diffusion of a JP in the laminar flow of eqn (1): D/D_L *vs.* D_θ/Ω_L for different values of v_0 (filled and empty symbols, see legends). We remind that here eqn (3) yields v_c = 0.4. Dashed curves represent the limiting cases $D = \kappa\sqrt{D_L D_0}$ (passive particle with Pe $\gg$ 1), $D = D_0 + D_s$ (free JP) and $D = \kappa\sqrt{D_L(D_0 + D_s)}$ (advection enhanced diffusivity of a JP in 2D[31]), with $D_s = v_0^2/2D_\theta$ (see text). Vertical arrows mark our estimates for D_θ^*, eqn (4), and a cross the maxima, D/D_L = 0.5, of the curves with $v_c < v_0 U_0$. Other simulation parameters are: D_0 = 0.01, U_0 = 1 and $L = 2\pi$, hence $D_L = \Omega_L$ = 1. A few curves for the same JP in the rigid-boundary flow of eqn (5) are plotted for a comparison (half-filled symbols of the corresponding shape and color).

and advection torque. The two, combined, optimize the mechanism of edge switching, whereby the JP moves from one pinning site at the bottom to a pinning site at the top, and *vice versa*. As such pinning sites are (at least) a distance $L/2$ apart, edge switching enhances lateral diffusion against edge pinning. Under these conditions (Fig. 4), the leading contribution to the diffusion constant is $D = (L/2\pi)^2\Omega_L/2$, *i.e.*, $D/D_L \simeq 1/2$, independent of v_0 and D_0 (Appendix A).

The curves for $v_0 \gg U_0$, as anticipated above, are mostly governed by self-propulsion. For a wide D_θ range, they closely follow the free diffusion law, $D = D_0 + D_s$, like in a straight zero-flow channel, even when $l_\theta > L/2$ (as a consequence of the reflecting boundaries). However, having chosen $D_0 \ll D_L$, at larger D_θ the JP free diffusion constant, $D_0 + D_s$, grows smaller than D_L: Particle's diffusion then takes place at effective high Péclet numbers and the advection enhanced diffusivity mechanism applies, hence $D = \kappa\sqrt{D_L(D_0 + D_s)}$.[31] These two distinct diffusion laws are both illustrated in Fig. 3 and 4.

All D curves with $v_0 > v_c$ in Fig. 4 share a surprising property: Upon lowering D_θ, they drop below the free diffusion value, D_0. This suggests that for $v_0 > v_c$ and large τ_θ advection at the array edges is never negligible. We already noticed that a JP with $l_\theta > L/2$ trapped at the array's edges can free itself either by sliding against the advection drag or by switching edge. We also know that in the limit D_0/D_L, $D_\theta/D_L \to 0$, a particle pointing against an edge with $|\cos\theta| < U_0/v_0$ ends up sitting in a stagnation corner, *i.e.*, sliding can be suppressed even for $v_0 \gg U_0$. Diffusion is then activated by autonomous edge switching, which, for a JP, can occur through either angular reorientation, with time constant τ_θ, or translational diffusion, with time constant $\tau_D = (L/2\pi)^2/2D_0$ (Appendix A). For $v_0 \gg U_0$, depinning from the edge washboard potential requires $|\theta| > U_0/v_0$, therefore, angular diffusion ceases driving edge switching when $2D_\theta\tau_D < (U_0/v_0)^2$, or $D_\theta < D_\theta^*$, with

$$D_\theta^*/\Omega_L = (U_0/v_0)^2(D_0/D_L). \quad (4)$$

As shown in Fig. 4, lowering D_0 below D_θ^* causes a sharp drop of the D curves to values so small that they could not be numerically computed with acceptable accuracy. This effect is clearly due to geometric confinement, as confirmed by the fact that it was never detected in 2D flows.[31]

5 Concluding remarks

We have investigated the diffusion of an active JP in a 1D array of counter-rotating convection rolls. The JP considered here should be regarded as modeling a self-propelling microswimmer of biological or synthetic nature, alike. Our choice for the laminar flow is meant to mimic the Rayleigh–Bénard rolls occurring between two parallel (free-slip) surfaces: by varying the temperature difference between them it is possible to vary the advection speed of the suspension fluid with respect to the speed of the active JP and thus explore the parameter space investigated in the present paper.

We focused on effects due the combination of three key ingredients, namely, thermal noise, advection and self-propulsion, in a confined geometry. Such effects, not detectable in 2D arrays of convection rolls with same hydrodynamical parameters but no boundaries, can be summarized as follows:

(i) The large-scale circulation of a JP trapped in a convection roll is confined to narrow flow boundary layers, whereby the particle self-propulsion velocity tends to line up with the advection drag, which results in an accumulation of the particle probability density.

(ii) The diffusion of an active JP with low self-propulsion speed is governed by its circulation along the roll boundaries, and is thus undistinguishable from that of a regular passive particle.

(iii) For larger self-propulsion speeds, the JP tends to sojourn in the vicinity of the array's edges and diffuses by sliding along them. Its diffusion is dominated by the advection drag parallel to the array's boundaries even for self-propulsion speeds much larger than the advection drag. This mechanism works for strengths of the angular noise above a certain threshold; below that threshold, the particle's diffusion constant drops to vanishingly small values.

Our emphasis on the above confinement effects is motivated by the widespread interest in controlling transport of diluted active matter[3,4] in microfluidic circuits.[13]

To this regard we note that, due to the large variability of the advection parameters in actual Rayleigh–Bénard cells[14,25] [L and U_0 in the model of eqn (1)] and the self-propulsion mechanisms[5,8] [v_0 and D_θ in the JP model of Section 2], all three diffusion regimes listed above are experimentally accessible. Both organic and synthetic microswimmers could be employed to investigate advection effects on the active diffusion in laminar flow patterns. Next focus of the present project is the self-assembly of advected JPs. Indeed, mixtures of both passive and active JPs are known to form a variety of superstructures[2–4] mostly because of of the hydrodynamic effects associated with the particle self-propulsion and the particle–particle interactions, all effects which have been neglected in this first report.

Finally, we remark that the overall picture presented here holds for rigid (or no-slip) boundary arrays, as well. Numerical results for the stream function,

$$\psi(x,y) = (U_0L/2\pi)\sin(2\pi x/L)\sin^2(2\pi y/L), \quad (5)$$

are reported in Fig. 3 and 4 for a comparison. The breakdown of the FBL circulation with increasing v_0 is still detectable, though not as sharp as in free-boundary convection arrays. In Fig. 3 the dips of the D curves occur at lower values of v_0 and are less pronounced. This happens because a particle moving against the edges of the array of eqn (5) is advection free: it moves subjected to the sole thermal noise; correspondingly, the FBL width shrinks. For the same reason, in Fig. 4 the D curves never drop below D_0.

Conflicts of interest

There are no conflicts to declare.

Appendix

A Model's time scales

The diffusion process of eqn (2) is characterized by many dynamical parameters. In particular, in our analysis of the diffusion data we made use of various time scales, which we now recap for reader's convenience, with reference to the underlying dynamical mechanisms:

(i) Angular diffusion. In eqn (2), the self-propulsion velocity vector, $\vec{v}_0$, was assumed to have constant modulus, v_0, and fluctuating orientation with angle $\theta(t)$. In the absence of advection, $U_0 = 0$, we know that,[10,38] $\langle v_i(t)v_i(0)\rangle = (v_0{}^2/2)\exp(-D_\theta|t|)$, with $i = x,y$. These autocorrelation functions prove that the angular noise strength, D_θ, plays the role of angular diffusion rate and, accordingly,

$$\tau_\theta = 1/D_\theta, \quad (6)$$

defines the persistence time of the ensuing active Brownian motion of the self-propelling JP.

(ii) Roll circulation. Due to advection, a particle trapped in a convection roll, is dragged along a circular FBL of approximate radius $L/4$ with speed U_0. This means that the particle circulates inside the trapping roll with period of the order of $\tau_L' = \pi L/2U_0$ or, equivalently, angular frequency $\Omega_L' = 4U_0/L = (2/\pi)\Omega_L$. Therefore, consistently with the current literature, we agreed to use the standard definition of circulation time scale,[35] namely

$$\tau_L = 2\pi/\Omega_L = L/U_0. \qquad (7)$$

(iii) Thermal diffusion. Subjected to thermal noise, the suspended particle diffuses across the array with mean first-passage time[1] $\tau_D' = (L/2)^2/2D_0$. Advection drag and thermal diffusion are comparable when $\tau_D'/\tau_L' \sim 1$. In the text, this condition has been reformulated more conveniently as $\Omega_L\tau_D \sim 1$, with

$$\tau_D = (L/2\pi)^2/2D_0. \qquad (8)$$

(iv) Ballistic self-propulsion. In the absence of angular diffusion, $D_\theta = 0$, the JP crosses ballistically a unit flow cell with time constant $\tau_0' = L/\langle|v_x|\rangle = \pi L/2v_0$. In this regime, the action of advection and self-propulsion are comparable under the condition that $\tau_0' \sim \tau_L'$, or, equivalently, $\tau_0 \sim \tau_L$, with

$$\tau_0 = L/v_0. \qquad (9)$$

It should be noted that ballistic effects due to self-propulsion are negligible with respect to advection and the array's geometry, respectively under the conditions $\Omega_L\tau_0 \gg 1$ and $D_\theta\tau_0 \gg 1$, that is, for $v_0 \ll U_0$ and $D_\theta/\Omega_L \gg v_0/U_0$.[31]

Eqn (6)–(9) define the time scales used in our analysis of the simulation data displayed in Fig. 3 and 4. They can also be combined to obtain convenient estimates of the reference diffusion scales introduced in Section 4. Firstly, based on our derivation of Ω_L', the diffusing particle is advected across the array width $L/2$ with effective speed $(2/\pi)U_0$.[39] This means that by hitting the roll boundaries it undergoes a large-scale diffusion with diffusion constant $D = (1/2)(L/2)(2U_0/\pi) = D_L$, which coincides with the diffusion scale associated with the stream function of eqn (1). Secondly, in Section 3, the FBL of a convection roll has been modeled as an annulus of radius $L/4$ and width $\delta = (D_0/\Omega_L)^{1/2}$; accordingly, it covers a fraction $\phi = 2\pi\delta/L$ of the roll's surface. We know that, for $v_0 < v_c$, the large-scale diffusion of a JP, with diffusion constant D_L, is restricted to the FBL network. Therefore, its effective diffusion constant is $D = \phi D_L$, that is, $D = \sqrt{D_L D_0}$. This simple argument reproduces the result of ref. 19 with $\kappa = 1$ instead of the more accurate $\kappa = 1.07$.

B Transverse distributions

We present in Fig. 5 the transverse distributions, $p(y)$, corresponding to the longitudinal distributions, $p(x)$. Combined with Fig. 1(c), (d) and 2 of Section 3, this figure illustrates the large-scale circulation of a JP with $v_0 < v_c$ and the break-up of the FBLs for $v_0 > v_c$. The depletion of the inner region of the convection rolls is the most pronounced for $v_0 \simeq U_0$ [Fig. 5(a)], which corresponds to the strongest interplay of advection and self-propulsion. In Fig. 5(d), the FBL break-up causes the sharp jumps of $\langle|\cos(2\pi y/L)|\rangle$, from 0 to 1 at $v_0 \sim v_c$.

Moreover, we stated in Section 3 that the flattening of the $p(x)$ for $v_0 \gg U_0$ is due to the symmetric particle accumulation against both array's edges. That statement is supported here by the profile of the corresponding $p(y)$ curves of Fig. 5(a), which, indeed, exhibit sharp maxima at $y = 0$ and $y = L/2$.

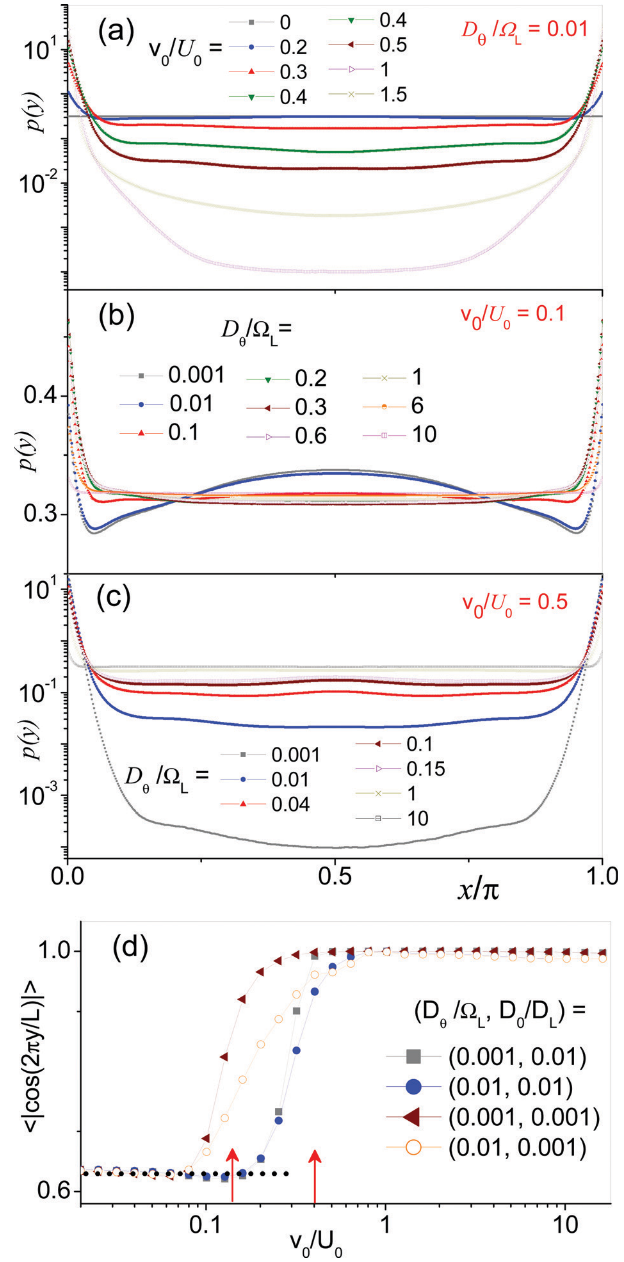

Fig. 5 Stationary transverse distributions: (a)–(c) transverse density functions, $p(y)$, corresponding to the longitudinal distributions, $p(x)$, of Fig. 2; (d) $\langle|\cos(2\pi y/L)|\rangle$ *vs.* v_0/U_0. Simulation parameters in (a)–(c) are the same as in the corresponding panels of Fig. 2; if not specified otherwise in the legend, the same parameters have been adopted in (d). Vertical arrows mark our estimates for v_c at $D_0 = 0.01$ and 0.001, eqn (3).

We remind once again that the nonuniform distributions $p(x)$ and $p(y)$ are peculiar of 1D convection arrays. Indeed, particle accumulation inside the FBLs for $v_0 < v_c$ and against the array's edges for $v_0 > v_c$ is an effect of geometric confinement. Numerical simulations of an active JP in the 2D flow of eqn (1), with periodic boundary conditions in the x and y direction, returned uniform longitudinal and transverse distribution for any value of v_0 (not shown).

C The role of thermal noise

For brevity, in Sections 3 and 4 we did not dwell on the role thermal noise. We just stressed that its strength, D_0, was set much smaller than the advection diffusion scale, D_L. Accordingly, we defined the Péclet number as $Pe = D_L/D_0$. We then mentioned that D_0 enters our estimates of both the FBL width, $\delta = (D_0/\Omega_L)^{1/2}$, and the break-up threshold, v_c, in eqn (3).

To support those statements we present here simulation results for the 1D distributions, $p(x)$ and $p(y)$, and the asymptotic diffusion constant, D, obtained for a value of D_0 one order of magnitude smaller than in Fig. 2–4. On comparing Fig. 6(a) with Fig. 2(b), it is apparent that the FBL width shrinks with increasing D_0. Analogously, the existence of the threshold v_c and its dependence on D_0 are confirmed by the curves D *versus* v_0, in Fig. 7(a), and D *versus* D_θ, in Fig. 7(b) [see also Fig. 5(d)].

The overall behavior of the diffusion curves in Fig. 7 is consistent with that displayed in Fig. 3 and 4. For instance, in Fig. 7(b) all curves with $v_c < v_0 U_0$ attain the same maximum, $D/D_L \simeq 1/2$ at $D_\theta/\Omega_L = 1$, as in Fig. 4, *i.e.*, independently of D_0. However, a few differences are worthy to note: (i) diffusion in the pinning range, $v_c < v_0 U_0$, of Fig. 7(a) reveals additional details, which went unnoticed in Fig. 3; (ii) these details reflect into the non-monotonic D_θ-dependence of the corresponding D curves in Fig. 7(b); (iii) The interplay between thermal, D_0, and angular noise, D_θ, causes the double-peaked aspect of the $p(x)$ maxima in Fig. 6(a) [absent in Fig. 2(b)]. These details do not affect the main conclusions of our work. We also remark here that obtaining simulation data with a good statistics at very low noise levels, $D_0 \to 0$ and (or) $D_\theta \to 0$, would require exceeding computational resources. For this reason we could not push our numerical investigation to lower D_0 values.

A more substantial difference between Fig. 4 and 7(b) regards the curves with $v_0 \gg U_0$. In Fig. 7(b) those curves seem to not bend downward upon decreasing D_θ. This is due to the fact that, consistently with eqn (4), for the simulation parameters of Fig. 7 the estimated position of their maxima, D_θ^* is not captured by the numerically accessible D_θ range.

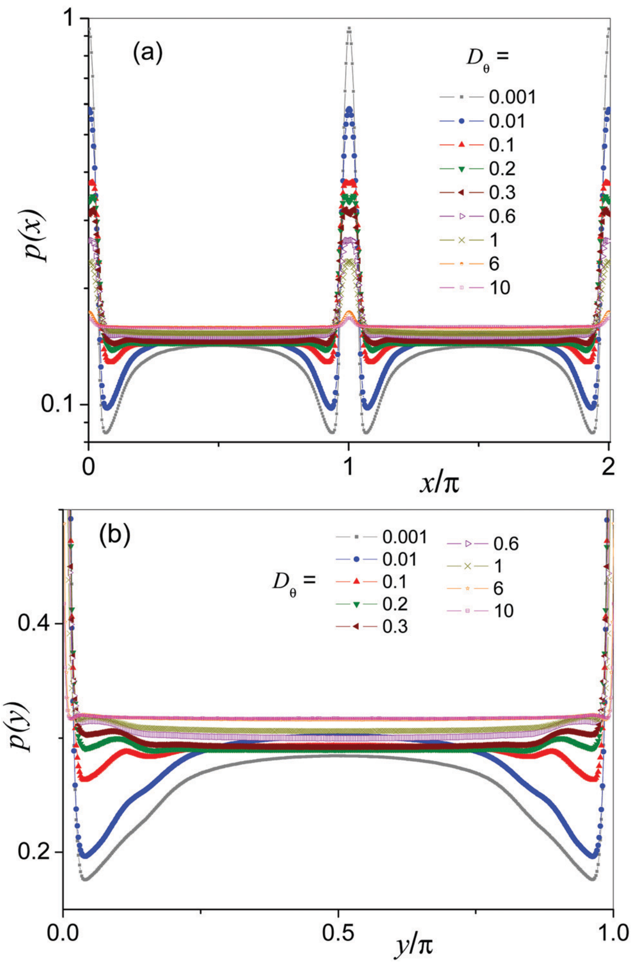

Fig. 6 Stationary distributions, $p(x)$ and $p(y)$, for different D_θ with the same simulation parameters as in panels (b) of Fig. 2 and 5, except for D_0 = 0.001. Note that here eqn (3) yields v_c = 0.13.

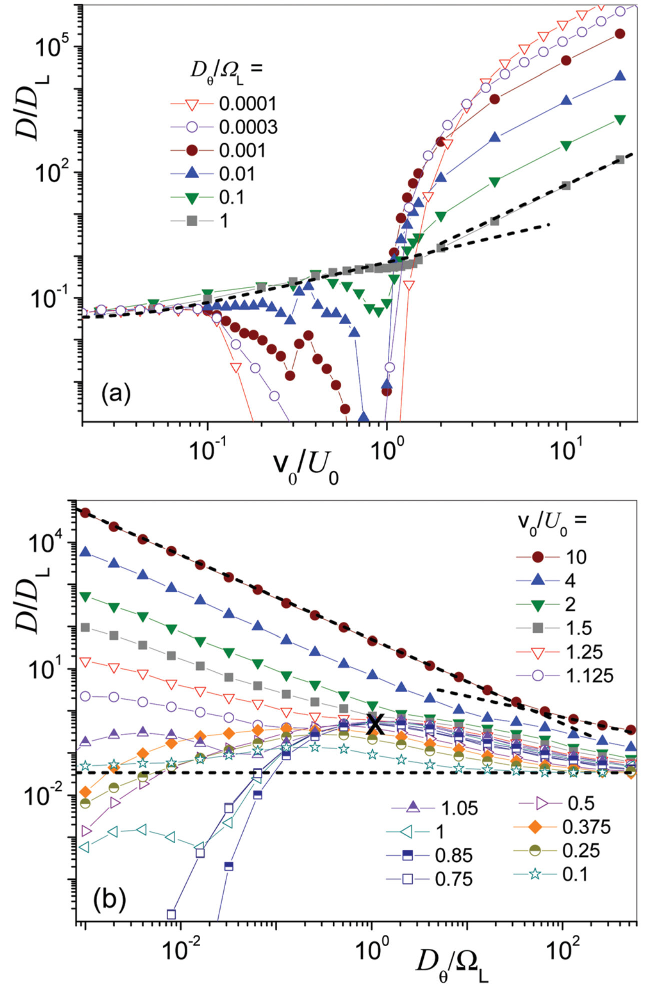

Fig. 7 Longitudinal diffusion of a JP in the laminar flow of eqn (1): same as in Fig. 3, (a), and Fig. 4, (b), but for D_0 = 0.001.

Acknowledgements

We thank RIKEN Hokusai for providing computational resources. Y. L. is supported by the NSF China under grants No. 11875201 and No. 11935010. P. K. G. is supported by SERB Start-up Research Grant (Young Scientist) No. YSS/2014/000853 and the UGC-BSR Start-Up Grant No. F.30-92/2015. F. N. is supported in part by: NTT Research, Army Research Office (ARO) (Grant No. W911NF-18-1-0358), Japan Science and Technology Agency (JST) (*via* the CREST Grant No. JPMJCR1676), Japan Society for the Promotion of Science (JSPS) (*via* the KAKENHI Grant No. JP20H00134 and the JSPS-RFBR Grant No. JPJSBP120194828), the Asian Office of Aerospace Research and Development (AOARD) (*via* Grant No. FA2386-20-1-4069), and the Foundational Questions Institute Fund (FQXi) *via* Grant No. FQXi-IAF19-06.

References

1 S. Redner, *A Guide to First-Passage Processes*, CUP, New York, 2001.
2 *Janus particle synthesis, self-assembly and applications*, ed. S. Jiang and S. Granick, RSC Publishing, Cambridge, 2012.
3 A. Walther and A. H. E. Müller, Janus particles: Synthesis, self-assembly, physical properties, and applications, *Chem. Rev.*, 2013, **113**, 5194.
4 M. C. Marchetti, J. F. Joanny, S. Ramaswamy, T. B. Liverpool, J. Prost, M. Rao and R. A. Simha, Hydrodynamics of soft active matter, *Rev. Mod. Phys.*, 2013, **85**, 1143.
5 J. Elgeti, R. G. Winkler and G. Gompper, Physics of microswimmers, single particle motion and collective behavior: a review, *Rep. Prog. Phys.*, 2015, **78**, 056601.
6 C. Bechinger, R. Di Leonardo, H. Löwen, C. Reichhardt, G. Volpe and G. Volpe, Active particles in complex and crowded environments, *Rev. Mod. Phys.*, 2016, **88**, 045006.
7 see e.g. *Smart Drug Delivery System*, ed. A. D. Sezer, IntechOpen, 2016, , DOI: 10.5772/60475.
8 J. Wang, *Nanomachines: Fundamentals and Applications*, Wiley-VCH, Weinheim, 2013.
9 A. M. Pourrahimi and M. Pumera, Multifunctional and self-propelled spherical Janus nano/micromotors: recent advances, *Nanoscale*, 2018, **10**, 16398–16415.
10 P. K. Ghosh, V. R. Misko, F. Marchesoni and F. Nori, Self-propelled Janus particles in a ratchet: Numerical simulations, *Phys. Rev. Lett.*, 2013, **110**, 268301.
11 D. Debnath, P. K. Ghosh, V. R. Misko, Y. Li, F. Marchesoni and F. Nori, Enhanced motility in a binary mixture of active nano/microswimmers, *Nanoscale*, 2020, **12**, 9717.
12 Q. Zou, Z. Li, Z. Lu and Z. Sun, Supracolloidal helices from soft Janus particles by tuning the particle softness, *Nanoscale*, 2016, **8**, 4070–4076.
13 B. J. Kirby, *Micro- and Nanoscale Fluid Mechanics: Transport in Microfluidic Devices*, Cambridge University Press, 2010.
14 P. Tabeling, Two-dimensional turbulence: A physicist approach, *Phys. Rep.*, 2002, **362**, 1.
15 X. Yang, C. Liu, Y. Li, F. Marchesoni, P. Hänggi and H. P. Zhang, Hydrodynamic and entropic effects on colloidal diffusion in corrugated channels, *Proc. Natl. Acad. Sci. U. S. A.*, 2017, **114**, 9564.
16 *Topological Aspects of the Dynamics of Fluids and Plasmas*, ed. H. K. Moffatt, G. M. Zaslavsky, P. Comte and M. Tabor, Springer, Netherlands, 1992.
17 S. Chandrasekhar, *Hydrodynamic and Hydromagnetic Stability*, Oxford University Press, New York, 1967.
18 For recent reviews on theory and experiments, see Dynamics of Spatio-Temporal Cellular Structures, *Springer Tracts in Modern Physics*, ed. I. Mutabazi, J. E. Wesfreid and E. Guyon, Springer, New York, vol. 207, 2006.
19 M. N. Rosenbluth, H. L. Berk, I. Doxas and W. Horton, Effective diffusion in laminar convective flows, *Phys. Fluids*, 1987, **30**, 2636.
20 A. M. Soward, Fast dynamo action in a steady flow, *J. Fluid Mech.*, 1987, **180**, 267.
21 B. I. Shraiman, Diffusive transport in a Rayleigh-Bénard convection cell, *Phys. Rev. A: At., Mol., Opt. Phys.*, 1987, **36**, 261.
22 W. Young, A. Pumir and Y. Pomeau, Anomalous diffusion of tracer in convection rolls, *Phys. Fluids*, 1989, **A1**, 462.
23 E. Bodenschatz, W. Pesch and G. Ahlers, Recent developments in Rayleigh-Bénard convection, *Annu. Rev. Fluid Mech.*, 2000, **32**, 709.
24 A. V. Getling, *Rayleigh-Bénard Convection*, World Scientific, Singapore, 1998.
25 T. H. Solomon and J. P. Gollub, Passive transport in steady Rayleigh-Bénard convection, *Phys. Fluids*, 1988, **31**, 1372.
26 T. H. Solomon and I. Mezić, Uniform resonant chaotic mixing in fluid flows, *Nature*, 2003, **425**, 376.
27 J.-A. Arguedas-Leiva1 and M. Wilczek, Microswimmers in an axisymmetric vortex flow, *New J. Phys.*, 2020, **22**, 053051.
28 L. D. Rubio, M. Potomkin, R. D. Baker, A. Sen, L. Berlyand and I. S. Aranson, Self-propulsion and shear flow align active particles in nozzles and channels, *Adv. Intell. Syst.*, 2021, **3**, 2000178.
29 O. A. Croze, G. Sardina, M. Ahmed, M. A. Bees and L. Brandt, Dispersion of swimming algae in laminar and turbulent channel flows: consequences for photobioreactors, *J. R. Soc., Interface*, 2013, **10**, 20121041.
30 A. Théry, L. Le Nagard, J.-C. Ono-dit-Biot, C. Fradin, K. Dalnoki-Veress and E. Lauga, Self-organization and convection of confined magnetotactic bacteria, *Sci. Rep.*, 2020, **10**, 13578.
31 Y. Li, L. Li, F. Marchesoni, D. Debnath and P. K. Ghosh, Active diffusion in convection rolls, *Phys. Rev. Res.*, 2020, **2**, 013250.
32 C. Torney and Z. Neufeld, Transport and aggregation of self-propelled particles in fluid flows, *Phys. Rev. Lett.*, 2007, **99**, 078101.
33 A. Zöttl and H. Stark, Emergent behavior in active colloids, *J. Phys.: Condens. Matter*, 2016, **28**, 253001.
34 P. E. Kloeden and E. Platen, *Numerical Solution of Stochastic Differential Equations*, Springer, Berlin, 1992.

35 Q. Yin, Y. Li, F. Marchesoni, T. Debnath and P. K. Ghosh, Exit times of a Brownian particle out of a convection roll, *Phys. Fluids*, 2020, **32**, 092010.
36 H. Risken, *The Fokker-Planck Equation*, Springer, Berlin, ch. 11, 1984.
37 G. Debnath, F. Moss, T. Leiber, H. Risken and F. Marchesoni, Holes in the two-dimensional probability densities of bistable systems driven by strongly colored noise, *Phys. Rev. A: At., Mol., Opt. Phys.*, 1990, **42**, 703.
38 J. R. Howse, R. A. L. Jones, A. J. Ryan, T. Gough, R. Vafabakhsh and R. Golestanian, Self-motile colloidal particles: From directed propulsion to random walk, *Phys. Rev. Lett.*, 2007, **99**, 048102.
39 Q. Yin, Y. Li, F. Marchesoni, D. Debnath and P. K. Ghosh, Excess diffusion of a driven colloidal particle in a convection array, *Chin. Phys. Lett.*, 2021, **38**(4), 040501.